Received 15 April 2024; accepted 21 April 2024. Date of publication 25 April 2024; date of current version 16 May 2024.

Digital Object Identifier 10.1109/OJCOMS.2024.3393480

Revolutionizing Batteryless IoT Systems to Enhance Nonlinear Energy Harvesting Using RIS Active and Passive Elements

SHAKIL AHMED [1] **(Member, IEEE), AHMED E. KAMAL** [1] **(Fellow, IEEE), MOHAMED Y. SELIM** [1] **(Senior Member, IEEE), SAIFUR RAHMAN SABUJ** [2] **(Senior Member, IEEE), AND MASANORI HAMAMURA** [3] **(Member, IEEE)**

[1] Department of Electrical and Computer Engineering, Iowa State University, Ames, IA 50011 USA

[2] Department of Electrical and Electronic Engineering, Brac University, Dhaka 1212, Bangladesh

[3] School of Informatics, Graduate School of Engineering, Kochi University of Technology, Kami 782-8502, Japan

CORRESPONDING AUTHOR: S. AHMED (e-mail: shakil@iastate.edu)

A preliminary version of this paper was presented at IEEE MILCOM 2021 conference [DOI: 10.1109/MILCOM52596.2021.9653007].

ABSTRACT Enhancing Internet of Things (IoT) communications through Reconfigurable Intelligent Surfaces (RIS) necessitates novel approaches that go beyond the conventional deployment of passive elements. This paper introduces an efficient method to enhance IoT system performance by combining active and passive functionality in RISs: an active and passive integrated approach. One identified enhancement area is efficiently managing signal throughput and exchanges in IoT systems, which is essential for supporting numerous devices. For this challenge, we propose a thorough process model that describes channel gains, develops a nonlinear energy harvesting, and identifies device-to-device communication schemes without violating information causality. The innovative component of our work is the utilization and strategic application of RIS panels that benefit from the advantages of active and passive components synergism to solve thermal noise issues and optimize signal reflection and transmission. An advanced optimization mechanism is developed based on mixed-integer nonlinear programming: an enabling approach between performance efficiency and maximum service utilization. Our simulation analysis show that developed RIS panels optimize IoT system performance and surpass existing performance indicators in conventional RIS-less systems.

INDEX TERMS Batteryless IoT sensor, D2D communications, nonlinear energy harvesting model, RIS active and passive elements.

I. INTRODUCTION

THE ADVENT of next-generation wireless networks marks a significant shift in the proliferation of Internet of Things (IoT) devices, which is rapidly transforming the landscape of digital communication [1]. The convergence of cutting-edge wireless technologies and IoT facilitates seamless integration between the tangible and virtual realms, thus revolutionizing an array of domains from e-healthcare and autonomous vehicles to smart cities and residential ecosystems [2]. As projections indicate a staggering increase to 50 billion IoT sensors, the critical need for extensive and intelligent connectivity is undeniable–positioning it as the cornerstone for the successful deployment of these burgeoning technologies.

In reality, many IoT sensors are inherently portable due to their diverse applications, presenting the challenge of ensuring consistent and continuous operation. Recent trends show an exponential rise in the deployment of batteryless IoT (b-IoT) sensors [3], often in locations that are inaccessible and devoid of proximal power sources [4], further complicating their power supply. Consequently, a dependable energy source emerges as a pivotal factor for the uninterrupted functioning of b-IoT sensors. Traditional power solutions, such as batteries and solar panels, entail substantial installation and maintenance expenses. As the deployment of b-IoT sensors escalates, there is a corresponding surge in demand for wireless power transfer, an alternative to conventional power supplies. The visionary Nikola Tesla originally conceived the idea of wireless energy transfer, pioneering the principles of transmitting energy through the air and its conversion into usable direct current (DC) [5]. This vision laid the groundwork for developing state-of-the-art power supply techniques, including energy harvesting.

IoT sensors can capture energy directly from external radio frequency (RF) sources, such as neighboring base stations (BSs), which appears to be a viable solution to power the sensors among the various forms of energy harvesting techniques [6]. Moreover, IoT sensors consume considerable energy due to continuous services, which may reduce sensors' lifetime in an energy-constrained scenario. To counter the effect, harvesting energy from BS RF signals enhances the lifetime of IoT sensors by converting RF energy to electrical energy [7]. However, energy harvesting is not a straightforward process; instead, an enhanced channel gain is a significant requirement to overcome the complexity and ensure improved performance. Thanks to the reconfigurable intelligent surface (RIS), it can enhance the gains between nodes and address the challenges by adjusting the direction of incident signals in a controlled fashion. The RISs take the system's performance, including energy harvesting and node communications, to the next level. Therefore, the need for efficient channel gains to assist wireless communications motivates using RISs for forthcoming next-generation technology.

An RIS panel is a flat metasurface structure designed to control electromagnetic waves dynamically. It consists of individually configured elements that intelligently induce a specific phase change on reflected signals to facilitate wireless propagation. There are two types of RIS elements: passive and active. The RIS passive elements reflect the incident signals, while the active elements reflect and amplify the incident signals to the receiving nodes. Therefore, RIS panels make IoT systems energy efficient by reflecting and amplifying incident signals so that the destination nodes receive directional and stronger transmit signals. In our previous work, we completed the first exploratory studies focused on optimizing RIS active and passive elements to improve data rates and energy harvesting in b-IoT systems employing a linear energy harvesting model [8], [9]. As valuable as these fundamental works are, our current paper aims to go beyond them by exploring the nonlinear model of energy generation. We make this transition for various reasons, such as the nonlinear model enabling us to mirror energy transfer dynamics more accurately, as real-world energy transfer is only quasi-linear: actual energy conversion efficiency does not increase linearly with input power, as limited by the laws of physics and technological constraints [10].

In wireless communications systems, RIS panels often compensate for double-fading attenuation [11], [12], [13], [14], [15], [16]. However, deploying several RIS elements may lead to significant overhead, such as higher complexity and expensive maintenance, due to the power consumption of internal circuits. Moreover, optimizing the performance of RISs, which involves adjusting parameters like phase shift, reflection angle, and amplitude, is challenging due to the complexity of RIS panel properties. Fortunately, a combination of active and passive elements in RIS technology has emerged as a promising solution to overcome these challenges. By carefully balancing the number of active and passive elements, nonlinear energy harvesting and bit transmission can be significantly enhanced. However, achieving this balance is complicated by the thermal noise generated by RISs, which requires careful consideration during optimization. Unlocking the full potential of RIS technology in improving wireless communications systems' efficiency, including energy harvesting and data transmission, requires addressing these challenges through significant research efforts and innovative solutions. Therefore, further investigation is necessary to achieve optimal performance and maximize the benefits of RIS technology.

A. RELATED WORKS AND MOTIVATION

In recent years, researchers from the wireless communities have studied various essential aspects of IoT systems, including energy harvesting, bits transmission maximization, and enhancement of systems with/without the help of RIS panel [12], [13], [14], [15], [16], [17], [18], [19], [20], [21], [22], [23], [24], [25], [26], [27], [28], [29], [30], [31]. Particularly, [12], [13], [14], [15], [16], [17], [18], [19], [20] discussed the IoT systems and illustrated the importance and possible deployment of RIS. For example, a novel framework to support IoT data transmission from the BS to optimize the achievable rate was proposed in [12]. The authors in [13] claimed that harvesting energy from RF sources is optimal for low-power IoT sensors. The authors in [14] designed an energy harvesting model for low-power-consuming IoT sensors to investigate environmental monitoring systems. Another novel idea to power IoT sensors was proposed in [15], where the sensors harvested energy from nearby smart devices, such as smartphones. The authors in [16] investigated IoT systems where the energy between the sensors is shared.

The authors in [17] designed a cognitive radio network to maximize resource allocation, such as the transfer of information and energy efficiency. They considered a secondary user with an undefined backlog of traffic, which performed the error-free sensing function to maximize the resource allocation. An energy region was calculated for a wireless system. The authors looked at a transmitter, a decoder, and an energy harvesting device to find the optimum region among the nodes in an opportunistic mobile network. The authors in [18] expanded the model to maximize systems throughput for secondary users by considering transmission power using a stochastic approach. They assumed that the users harvested energy for another user if they resided close to each other. In [19], a wireless network was studied to maximize spectral efficiency by harvesting energy. The authors in [20] studied the features of the BS RF signals and microcontrollers for configuring the status of the RF systems for b-IoT sensors, which are energized using harvested energy to convert energy from an external source, for example, RF signals to DC energy. The concept of wireless energy transfer for IoT leverages electromagnetic fields to remotely power devices, a critical advancement for sustainable IoT ecosystems [21]. RF energy harvesting, a critical method in WET, transforms ambient RF signals into electrical energy, enabling batteryless operation of IoT devices [22], [23]. This foundational technology paves the way for deploying maintenance-free sensors and devices across diverse applications, driving innovations in IoT system design and energy efficiency [24]. The authors in [25] investigated the impact of renewable energy sources on power grid stability, highlighting the importance of integrating solar and wind power generation for sustainable energy systems. The authors in [26] addressed the minimum length scheduling problem in full-duplex model for massive machine-type communications, providing optimal and heuristic algorithms for discrete-rate transmission configurations.

The RIS panel has been proposed in various wireless network domains, such as IoT sensors, cognitive radio networks, device-to-device (D2D) communications, unmanned aerial vehicles (UAVs), etc. The possible deployment of the RIS panels integrated into IoT systems significantly enhances the system performance [21], [22], [23], [24], [25], [26], [27], [28], [29], [30]. For example, an RIS-assisted link between a BS and a user was considered to maximize the throughput by increasing the elements of the RIS panel in [27]. They also focused on maximizing energy efficiency in RIS-assisted wireless networks. An RIS-aided future wireless network was proposed in [28] for indoor and outdoor scenarios. The authors considered a single RIS panel to maximize the system performance matrices. The authors in [29] studied relay-based wireless networks with the help of the RIS panel. In their proposed networks, the RIS panel enhanced the link between transmitter and receiver in the first hop, while the other hop was enhanced by relay. The required channel state information estimation was considered in [30] by embedding RIS active sensors.

The authors in [31] used the Fisher-Snedecor F model to estimate the channel in the RIS panel-assisted wireless networks. The mean square error for RIS panel-assisted IoT systems was investigated in [32] to minimize the mean square error in their model. The authors in [33] investigated a rate maximization problem using the RIS panel and UAV. While energy harvesting from RF sources has been widely studied, most research is limited to decoding information with a nonlinear energy harvesting model [34], [35]. A framework for RIS panel-assisted low-power IoT systems was studied to investigate the back-scatter communications in [36]. The authors proposed a spectrum sensing algorithm using RISs offering significant gain compared to conventional sensing without RIS [37]. Unfortunately, none of the works in [12], [13], [14], [15], [16], [17], [18], [19], [20], [21], [22], [23], [24], [25], [26], [27], [28], [29], [30], [31] explored the potential RIS active and passive elements benefits for improving the b-IoT systems' performance.

B. CONTRIBUTIONS

We focus on enhancing the efficiency of RIS-supported wireless networks specifically designed for b-IoT sensors. *To the best of our knowledge, this is the first instance of such an endeavor.* Our noteworthy contributions are outlined below:

- *Optimal nonlinear energy harvesting with RIS:* First, we use a nonlinear model to identify the optimal energy harvesting model from the BS RF signals in the first optimal time slot within a specified given time frame. Then, we optimize the energy consumption and data transmission between the BS and b-IoT sensors by utilizing the harvested energy. We achieve this by determining the optimal number of RIS active and passive elements to overcome network fading or shadowing. We are the first to consider a practical scenario that combines a nonlinear energy harvesting model with RIS active and passive elements while considering the RIS-generated thermal noise. Our research contributes significantly to the literature by providing a design approach for optimal nonlinear energy harvesting model with RIS elements and ensuring improved performance in b-IoT systems.
- *Optimal D2D communications with RIS:* Using the harvested energy and D2D communications protocol, we aim to maximize the number of bits transmission while adhering to the information causality constraint. This constraint guarantees the information is forwarded from the BS to the next IoT sensor. To achieve this, we also determine the optimal number of RIS elements required for efficient D2D communications.
- *RIS thermal noise and performance trade-off:* As the number of RIS active elements increases, the thermal noise also increases, causing the signal-to-noise ratio (SNR) to no longer be an increasing function. To address this issue, we establish a trade-off between the number of RIS elements and the system performance, considering the impact of RIS thermal noise on both energy harvesting and D2D communications phases. We achieve optimal performance while ensuring affordable overhead, such as hardware complexity and cost.
- *Efficient algorithm and performance evaluation:* We jointly optimize the communications time, and BS power budget, and RIS elements. We tackle the non-convex mixed-integer nonlinear programming (MINLP) optimization problem through an efficient iterative algorithm. Our results demonstrate that RIS-assisted systems outperform conventional wireless networks. After comparing the resources utilized in the energy harvesting and D2D communications phases, we observed that energy harvesting requires more RIS elements than

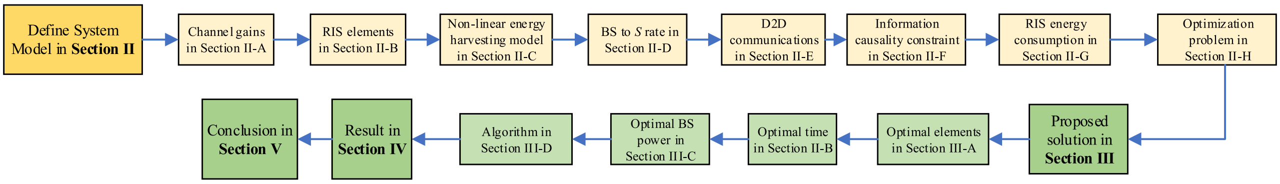

FIGURE 1. Paper organization.

D2D communications. The results of our study indicate that significant improvements can be achieved by using an optimal number of RIS elements.

C. NOTATIONS AND PAPER ORGANIZATION

We distinguish scalar, vector, and matrix with the variables a, $\mathbf{a}$, and $\mathbf{A}$, respectively. We also define $[\cdot]^*$, $[\cdot]^\dagger$, and $[\cdot]^f$ as optimal values, conjugate transpose, and feasible points, respectively. Fig. 1 shows the flow diagram of the paper organization. We define the proposed system model with a detailed description of RIS with elements-assisted networks in Section II. The proposed optimal element finding is illustrated in Section III. While the results are shown in Section IV, we conclude in Section V.

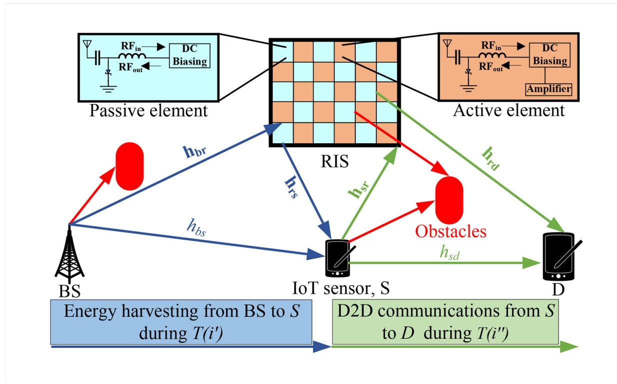

FIGURE 2. System model with RIS elements. Light blue for passive and light brown for active RIS tiles indicate their distribution, directly impacting the system's energy efficiency and signal enhancement in our results.

II. SYSTEM MODEL

In this study, 'batteryless' stands for IoT sensors that rely on nonconventional or pre-installed batteries for electrical power. Batteryless sensors are designed to gather energy from their surroundings or other sources, such as radio frequency signals, to power their operations. This lack of conventional batteries helps them become self-sustaining for relatively long periods. To operate at two slots of time, one each for energy harvesting and transmitting information, the authors have introduced an energy storage element, for instance, a capacitor or supercapacitor, in the sensor's design. During the first time slot, the sensor stores energy gathered from external sources, such as RF signals directed to it from a base station using its energy harvester circuit. This energy is stored and used during a second time slot to transmit information. By designing them to work in two different time slots without which the sensor lacks electric energy, it is ensured that they never run out of energy while also making the sensor self-regulating. This design is crucial in ensuring that batteryless IoT systems become the best option for sensor network operation, especially when the users lack resources or expertise for their maintenance.

Modeling a single-antenna base station was a conscious simplification in our choice to examine the effect of the RIS on enhancing batteryless IoT performance. This is representative of scenarios involving low-complexity or cost-sensitive networks, rendering our findings applicable to a wide range of real-world environments. By introducing such a straightforward scenario, we determine the RIS's potential to enhance connectivity, which is relevant even to circumstances where multi-antenna infrastructure is unattainable. From this point, our future work will advance our model to include base stations with several antennas, replicating more standard implementations while maintaining the similitude to MIMO systems in actual deployment.

We investigate IoT systems consisting of BS and IoT sensors, S and D, communicating in RIS-assisted wireless networks. The BS and IoT sensors are equipped with a single antenna. We deploy an RIS panel in the network to improve the system's performance. We aim to minimize the RIS energy consumption while maximizing the number of bits transmitted. We achieve this objective by employing an RIS panel equipped with active and passive elements, as illustrated in Fig. 2. The BS is considered to have single antenna elements, while each sensor has a single antenna.

We design a wireless system where the total time is a repetition of the time frame. We define i as the frame number while i', and i'' are the slots of frame i. The duration of frame, i, is $T(i)$ which is divided two slots with duration $T(i')$ and $T(i'')$. We also assume the coherence time is much longer than $T(i)$; hence, the channel conditionals within $T(i)$ are quasistatic. The RIS panel consists of N elements with m active and k passive elements, where $m+k \leq N$. The RIS panel assists the IoT sensor, S, to harvest energy from the BS RF signals in $T(i')$ and also in D2D communications from S to D in $T(i'')$. We use a nonlinear model for energy harvesting from the BS RF signals. S communicates to D during $T(i'')$. The model enforces the information causality constraint to forward the information received from the BS to another IoT sensor, D. Finally, we optimize overall RIS energy consumption and number of bits transmission during $T(i)$. We focus on finding the optimal number of elements, given by m^* and k^*, respectively, during $T(i)$. Table 1 displays the mathematical notations utilized in the paper.

A. CHANNEL GAINS

Without loss of generality, we assume that the channel gains are the same during each transmission frame with noise variance. The gains from S to D, BS to S, BS to RIS, RIS to S, S to RIS, and RIS to D are defined as h_{sd}, h_{bs}, $\mathbf{h_{br}} \in \mathbb{C}^{N\times 1}$, $\mathbf{h_{rs}} \in \mathbb{C}^{1\times N}$, $\mathbf{h_{sr}} \in \mathbb{C}^{N\times 1}$, and $\mathbf{h_{rd}} \in \mathbb{C}^{1\times N}$, respectively. The channel gains of the communications links from BS to S and S to D are modeled using Rician fading and, respectively, are given as follows:

$$h_{bs} = \frac{\sqrt{\beta_{bs}^{-1}}}{\sqrt{\Upsilon_e + 1}}\left(\sqrt{\Upsilon_e} h_{bs}^{los} + h_{bs}^{nlos}\right), \tag{1}$$

$$h_{sd} = \frac{\sqrt{\beta_{sd}^{-1}}}{\sqrt{\Upsilon_s + 1}}\left(\sqrt{\Upsilon_s} h_{sd}^{los} + h_{sd}^{nlos}\right). \tag{2}$$

where $\beta_{bs} = \frac{16\pi^2 d_1^{\delta_1}}{\lambda^2}$ and $\beta_{sd} = \frac{16\pi^2 d_2^{\delta_2}}{\lambda^2}$. λ is the wavelength. δ_1^p and δ_2^p are the path loss exponent. d_1 and d_2 are communicating node distance. The elements of h_{bs}^{nlos}, h_{bs}^{los}, h_{sd}^{nlos}, and h_{sd}^{los} are independently and identically distributed according to $\mathcal{CN}(0, 1)$. $\Upsilon_{\{e,s\}} \in [0, +\infty)$ is Rician factor.

TABLE 1. List of mathematical symbols.

Symbol	Description	Symbol	Description
		Constants	
$f_{\{.\}}$	Constant	$T(i^{'})$	Energy harvesting time
λ	Wavelength	$T(i^{''})$	D2D communications time
$\mathcal{O}$	Complexity	N	RIS elements
z_1	Noise	p_{sc}	Switch/control power
p_{dc}	DC power	a_m	Amplification factor
$W_{\{.\}}$	Bandwidth	$\delta_{\{.\}}$	Path loss component
$h_{\{.\}}$	Gains	ζ	Efficiency factor
$\mathbf{h_{rd}}$	RIS-D gain	α_i, β_i	Reflection coefficient
$\mathbf{h_{sr}}$	S-RIS gain	S	Unit power signals
$\Upsilon_{\{.\}}$	Rician factor	$Y, y_{\{.\}}$	Constants
h_{bs}	BS-S gain	$T(i)$	Time duration for frame, i
$\mathbf{h_{br}}$	BS-RIS gain	h_{sd}	S-D gain
$\mathbf{h_{rs}}$	RIS-S gain	$\mathbf{z_2}$	RIS thermal noise
$d_{\{.\}}$	Distance	$p_{out,m}$	Active elements output power
$\sigma^2_{\{.\}}$	Overall noise	$p_{in,m}$	Active elements input power
		Variables	
m	Active elements	$p_{ct}(i)$	Active element power at slot i
k	Passive elements	$p_{ss}(i)$	Passive element power at slot i
p_b	BS power	$s_{\{.\}}$	Received signal
$\mathbf{\Theta},\mathbf{\Phi}$	RIS phase shifts	p_{nl}	Harvested power
e_{nl}	Harvested energy	B_b	Number of BS-S bits
$[\cdot]^f$	Feasible point	B_d	Number of S-D bits
e_r	element energy	R_d	S-D rate
p_{nl}	Harvested power	R_b	BS-S rate
$[\cdot]^*$	Optimal value	e_{nl}	Harvested energy

B. RIS WITH ACTIVE AND PASSIVE ELEMENTS

1) THE CONTROLLING OF RIS PANEL

The RIS updates its configuration states from one to the next by receiving external commands via either a detached microcontroller architecture such as a field-programmable gate array (FPGA) or an integrated microcontroller architecture like a network of communicating chips/elements [38]. FPGA-based architectures are typically bulky and consume a significant amount of power. On the other hand, the integrated architecture uses a network of communicating chips/element to read the state of the elements and adjust the bias voltages using impedance-adjusting semiconductors. These circuits receive, interpret, and apply the commands while exhibiting static and dynamic power consumption [39].

The authors in [40] suggested that these integrated microcontrollers could work autonomously by harnessing energy from nano-networking advancements and using asynchronous logic, eliminating the need for complex and power-consuming clock distributions. Using integrated architecture, this control method provides amplitude measurements of reflection coefficients at a given frequency and is more efficient than the near-field model. This design improves performance while reducing hardware complexity and cost by reducing the microcontrollers needed to control multiple RIS elements. The passive elements reflect incident signals, and active elements amplify them, leading to additional energy consumption related to DC circuit power dissipation.

A wavelength is larger than a single RIS element, which can be as small as $\frac{\lambda}{8} \times \frac{\lambda}{8}$. The RIS elements scatter the signal with approximately equal gain towards the receiving nodes. As shown in Fig. 2, the RIS panel consists of N elements. m and k represent the active and passive elements, respectively. We use $m(i') \le m$ and $k(i') \le k$ during $T(i')$ while $m(i^{''}) \le m$ and $k(i^{''}) \le k$ are used during $T(i^{''})$. For a total number of elements, $(m + k)$, the RIS panel has the following number of elements used in energy harvesting and data transmission phases during the first and second time slots, respectively, as follows:

$$m + k \le N. \tag{3}$$

2) ENERGY HARVESTING FROM BS RF SIGNALS

During the energy harvesting phase, the amplitude and phase shift introduced by the RIS panel elements are encapsulated within an $N \times N$ diagonal matrix. This matrix is defined as:

$$\mathbf{\Theta} = \mathrm{diag}\Big(\alpha_1 e^{j\theta_1}, \alpha_2 e^{j\theta_2}, \ldots, \alpha_k e^{j\theta_k}, \alpha_{k+1} e^{j\theta_{k+1}}, \alpha_{k+2} e^{j\theta_{k+2}}, \ldots, \alpha_N e^{j\theta_N}\Big). \tag{4}$$

The fixed amplitude reflection coefficient for the RIS elements is denoted by α. For passive elements, indexed by $i = 1, 2, \ldots, k$, the reflection coefficient α_j is constrained to the interval [0, 1]. In contrast, for active elements, identified by indices $j = k + 1, k + 2, \ldots, N$, the coefficient is set to $\alpha_j \ge 1$. Additionally, the phase shift introduced by each RIS element is represented by θ, with $\{\theta_1, \theta_2, \ldots, \theta_k\}$ specifying the phase shifts for passive elements and $\{\theta_{k+1}, \theta_{k+2}, \ldots, \theta_N\}$ for active elements.

3) DATA TRANSMISSION

The IoT sensor, S, communicates with another IoT sensor, D, using a D2D communications protocol. During the data transmission phase, the $N \times N$ diagonal matrix that describes the amplitude and phase shift introduced by the RIS panel elements is given as follows:

$$\mathbf{\Phi} = \mathrm{diag}\Big(\beta_1 e^{j\phi_1}, \beta_2 e^{j\phi_2}, \ldots, \beta_k e^{j\phi_k}, \beta_{k+1} e^{j\phi_{k+1}}, \beta_{k+2} e^{j\phi_{k+2}}, \ldots, \beta_N e^{j\phi_N}\Big). \quad (5)$$

where the fixed amplitude reflection coefficient is defined as β. We limit $\beta_j \in [0, 1]$, where $i = 1, 2, \ldots, k$ for passive elements and $\beta_j \geq 1$, where $j = k+1, k+2, \ldots, n$ for active elements. The phase-shift of the RIS elements is defined as ϕ. We define $\{\phi_1, \phi_2, \ldots, \phi_k\}$ for passive elements and $\{\phi_{k+1}, \phi_{k+2}, \ldots, \phi_N\}$ for active elements, respectively.

C. NONLINEAR ENERGY HARVESTING MODEL

We use the complex nonlinear harvesting model to determine the optimal number of elements. This may necessitate incorporating more elements, i.e., in need of multiple elements, as we incorporate the information causality constraint in the system. The signal received from the BS to S is:

$$\begin{aligned} s_{bs}(i') &= \underbrace{\sqrt{p_b} h_{bs} s}_{\text{direct link}} + \underbrace{\mathbf{h_{rs}} \mathbf{\Theta}\big(\sqrt{p_b}\mathbf{h_{br}} s + \mathbf{z}_2\big)}_{\text{RIS-aided link}} + z_1, \\ &= \sqrt{p_b}(h_{bs} + \mathbf{h_{rs}}\mathbf{\Theta}\mathbf{h_{br}}) s + \mathbf{h_{rs}}\mathbf{\Theta}\mathbf{z}_2 + z_1. \end{aligned} \quad (6)$$

where S denotes the unit-power information signal, and $\mathbf{z_2} \in \mathbb{C}^{N\times 1}$ represents the generated thermal noise of the RIS panel during the energy harvesting from the BS RF signals with a distribution of $\mathcal{CN}(0, \sigma_2^2)$. The term z_1 denotes the additive Gaussian channel noise with a distribution of $\mathcal{CN}(0, \sigma_1^2)$. Given $\mathbf{\Theta}$, we can obtain the capacity of the additive white Gaussian noise channel with the channel gains as follows:

$$\mathbf{h_{rs}}\mathbf{\Theta}\mathbf{h}^{\dagger}_{\mathbf{rb}} = \sum_{n=1}^{N} \alpha_n e^{j\theta_n} [\mathbf{h_{rs}}]_n \Big[\mathbf{h}^{\dagger}_{\mathbf{rb}}\Big]_n, \quad (7)$$

The number of RIS elements is denoted by N. To achieve the maximum rate, θ_n should be selected optimally to maximize the sum of $\mathbf{h_{rs}}\mathbf{\Theta}\mathbf{h}^{\dagger}_{\mathbf{rb}}$. The expression for θ_n is given below:

$$\theta_n = \arg(\mathbf{h_{bs}}) - \arg\Big([\mathbf{h_{rs}}]_n \Big[\mathbf{h}^{\dagger}_{\mathbf{rb}}\Big]_n\Big), \quad (8)$$

The amount of energy harvested from BS RF signals during $T(i')$ using a nonlinear model can be described as shown in [41]:

$$e_{nl}\big(i'\big) = \frac{YT\big(i'\big)}{1 + \exp(-y_1(p_{nl}(i') - y_2))}, \quad (9)$$

where

$$p_{nl}\big(i'\big) = \zeta p_b \frac{\big(h_{bs} + (a_m m(i') + k(i'))h_1\big)^2}{\sigma_1^2}. \quad (10)$$

In this definition, $h_1 = [\mathbf{h_{rs}}]_n [\mathbf{h}^{\dagger}_{\mathbf{rb}}]_n$. a_m is the amplification factor. The active and passive elements used during $T(i')$ are represented by $m(i')$ and $k(i')$, respectively. $\zeta \in [0, 1]$ is the power split coefficient that indicates the portion of power assigned to the energy harvesting unit. Y, y_1, and y_2 define the various parameters required for the wireless energy harvesting model, where y_1 and y_2 capture the effects of resistance, capacitance, and circuit sensitivity [41]. Y represents a scaling factor that adjusts our model's overall energy harvesting capacity. It scales the output power to match realistic energy harvesting scenarios. y_1, y_2 are parameters designed to model the nonlinear characteristics of the energy harvesting process, where y_1 typically represents the impact of circuit resistance and y_2 encompasses the effects of capacitance and circuit sensitivity.

The parameters of our model are defined as follows: $p_{nl}(i')$ represents the effective power available for harvesting, factoring in the base station's transmit power p_b, the amplification factor a_m for active RIS elements, and the combined channel gain $h_{bs} + (a_m m(i') + k(i'))h_1$. Y scales the maximum harvestable energy within a time frame to the system's physical limits. y_1 and y_2 are model parameters that encapsulate the energy harvester's sensitivity to input power, embodying the effects of circuit resistance, capacitance, and intrinsic efficiency.

Empirical validation of this model involved comparing predicted harvested energy against measurements from prototype energy harvesters under varied RF conditions, demonstrating its accuracy across a wide range of power levels. Theoretical support is derived from the physics of semiconductor materials in rectifying antennas (rectennas), where the nonlinear diode rectification process exhibits a sigmoidal power response, which our model effectively captures. Our nonlinear energy harvesting model is theoretically sound and empirically validated through this comprehensive approach, offering a realistic representation of energy conversion dynamics in RIS-enhanced IoT systems.

D. DATA TRANSMISSION FROM BS TOS

We calculate the data rate transmission from the BS to S during $T(i')$ as follows:

$$\begin{aligned} R_b\big(i'\big) &= \max_{\theta_1,\ldots,\theta_N} W_1 \log_2\left(1 + \frac{p_b\Big(h_{bs} + \mathbf{h}_{\mathrm{rs}}\mathbf{\Theta}\mathbf{h}^{\dagger}_{\mathrm{rb}}\Big)^2}{\sigma_b^2}\right), \\ &= W_1 \log_2\left(1 + \frac{p_b\Big(h_{sd} + \Big(a_m m\Big(i'\Big) + k\Big(i'\Big)\Big)h_1\Big)^2}{\sigma_b^2}\right), \end{aligned} \quad (11)$$

where W_1 is the carrier frequency bandwidth. We define $\sigma_b^2 = \sigma_2^2 ||\mathbf{h_{rs}}\mathbf{\Theta}||^2 + \sigma_1^2$.

E. D2D COMMUNICATIONS

D2D communication is possible between devices due to direct wireless connections without a central network infrastructure layer, eliminating delays and saving energy. To allow multiple users to communicate seamlessly, our systems include a dynamic device detection and channel allocation process. Depending on the application's scope and power needs, we support a range of protocols, including Bluetooth low energy for close-range communication and LoRa for long-range communication. That flexibility will allow our systems to adapt to various environments in which our systems need to be operational, enabling D2D cooperation to deliver optimal overall performance. The received signal at sensor, D during $T(i^{''})$ from b-IoT sensor, S is expressed as follows:

$$s_{bs}\left(i''\right) = \underbrace{\sqrt{\frac{e_{nl}(i')}{T(i'')}} h_{sd} s}_{\text{direct link}} + \underbrace{\mathbf{h_{rd}} \mathbf{\Phi} \left(\sqrt{\frac{e_{nl}(i')}{T(i'')}} \mathbf{h_{sr}} s + \mathbf{z}_2 \right)}_{\text{RIS-aided link}} + z_1,$$
$$= \sqrt{\frac{e_{nl}(i')}{T(i'')}} (h_{sd} + \mathbf{h_{rd}} \mathbf{\Phi} \mathbf{h_{sr}}) s + \mathbf{h_{rd}} \mathbf{\Phi} \mathbf{z}_2 + z_1, \quad (12)$$

For given $\mathbf{\Phi}$, the gains are defined as follows:

$$\mathbf{h_{rd}} \mathbf{\Phi} \mathbf{h}_{\mathbf{rs}}^{\dagger} = \sum_{n=1}^{N} \beta_n e^{j\phi_n} [\mathbf{h_{rd}}]_n \left[\mathbf{h}_{\mathbf{rs}}^{\dagger}\right]_n, \quad (13)$$

We can express $\mathbf{h}_{\mathbf{rs}}^{\dagger}$ as the conjugate transpose of $\mathbf{h_{rs}}$. To achieve the maximum rate using $\mathbf{h_{rd}} \mathbf{\Phi} \mathbf{h}_{\mathbf{rs}}^{\dagger}$, we select ϕ_n to maximize the sum, which is the same phase as h_{sd}. Thus, we can calculate ϕ_n as $\phi_n = \arg(h_{sd}) - \arg([\mathbf{h_{rd}}]_n [\mathbf{h}_{\mathbf{rs}}^{\dagger}]_n)$. To calculate the rate during $T(i^{''})$ using harvested energy, we use the following formula:

$$R_d\left(i''\right) = \max_{\phi_1, \ldots, \phi_N} W_2 \log_2 \left(1 + \frac{\frac{e_{nl}(i')}{T(i'')} \left(h_{sd} + \mathbf{h}_{\text{rd}} \mathbf{\Phi} \mathbf{h}_{\text{rs}}^{\dagger} \right)^2}{\sigma_d^2} \right),$$
$$= W_2 \log_2 \left(1 + \frac{\frac{e_{nl}(i')}{T(i'')} \left(h_{sd} + \left(a_m m\left(i^{''}\right) + k\left(i^{''}\right)\right) h_2 \right)^2}{\sigma_d^2} \right). \quad (14)$$

where the carrier bandwidth is defined as W_2. We define $h_2 = [\mathbf{h_{rd}}]_n [\mathbf{h}_{\mathbf{rs}}^{\dagger}]_n$ and $\sigma_d^2 = \sigma_2^2 ||\mathbf{h_{rd}} \Phi||^2 + \sigma_1^2$.

F. INFORMATION CAUSALITY CONSTRAINT

The BS sends information to S in $T(i')$ time, which is then forwarded to D in $T(i^{''})$. The information causality constraint ensures that S forwards to D only the received information from the BS. The information causality constraint is:

$$T\left(i'\right) W_1 \log_2 \left(1 + \frac{p_b \left(h_{sd} + (a_m m(i^{'}) + k(i^{'})) h_1 \right)^2}{\sigma_b^2} \right)$$
$$\leq T\left(i''\right) W_2 \log_2 \left(1 + \frac{\frac{e_{nl}(i')}{T(i'')} \left(h_{sd} + \left(a_m m\left(i^{''}\right) + k\left(i^{''}\right)\right) h_2 \right)^2}{\sigma_d^2} \right). \quad (15)$$

G. RIS PANEL ENERGY CONSUMPTION

This section focuses on calculating the energy consumption of the RIS elements by considering both the energy harvesting and data transmission phases. The energy consumption in the passive elements is primarily due to the circuits related to the switch and control. On the other hand, active elements have a higher energy consumption because of the power consumed by the active loads and power amplification, in addition to the energy consumed by the switch and control circuits.

1) PASSIVE ELEMENTS POWER CONSUMPTION

Recall that k is the number of RIS passive elements. We express the RIS power consumption due to passive elements as follows:

$$p_{ss}(i) = k(j) p_{sc} \text{ for } j \in \left\{i', i''\right\}, \quad (16)$$

where p_{sc} is the energy consumption of each element, considering switch and control circuits.

2) ACTIVE ELEMENTS POWER CONSUMPTION

The focus of analyzing the active elements' energy consumption is on the DC circuit loss and the output power. The RIS active elements amplify reflected signals with negative resistance tunnel diodes and a DC polarization source, leading to power loss in the DC circuit. The output power encompasses the energy consumption by the switch and the control circuit. To get a reasonably tractable and accurate power consumption model, the power amplifier model from [42] is used to characterize the power consumption of the reflection amplifier for active elements. The power consumed by m number of identical active elements during energy harvesting is:

$$p_{ct} = m(p_{ss} + p_{dc}) + f\left(p_{out,m}\right), \quad (17)$$

The RIS active elements' power consumption is analyzed with a focus on the power dissipation caused by the DC circuit loss and the output power. The output power includes the energy consumed by both the switch and control circuit, represented by p_{ss}, and the DC biasing power consumption, represented by p_{dc}, which can be expressed as the sum of these two, i.e., $(p_{ss} + p_{dc})$. The output power dependent term, $f(p_{out,m})$, is determined by the output power, $p_{out,m}$ for m number of active elements. This term can be modeled linearly through empirical expression as follows [43]:

$$f\left(p_{out,m}\right) = \frac{p_{out,m}}{v} = \frac{a_m^2 p_{in,m}}{v}, \quad (18)$$

The output power for m number of active elements is related to the incident signal power $p_{in,m}$ through the amplifier efficiency, v. This relationship can be expressed as follows:

$$p_{in,m} = ||\mathbf{h_{br}}||^2 p_b + \sigma_2^2, \tag{19}$$

The reflection amplifier operates in a linear region where output power is proportional to input power, particularly for tunnel diode-based reflection amplifiers with inputs within their operational range [44]. The attenuation of the BS-RIS channel may weaken the transmitted signal, providing a high amplification gain for the reflection amplifier with low output power. Most studies only consider DC power consumption when estimating power consumption as output amplification power typically comprises a minor component of the total power consumption compared to DC power consumption [45]. The active elements in RIS provide signal amplification, reducing power consumption without requiring complex and power-hungry RF components. The power consumption of reflection amplifiers has been reduced to μW. The system benefits from the active elements in the RIS by improving signal combination at the receiver and increasing power amplification.

Power consumption during energy harvesting: Using (17)-(19) the power consumption expression is:

$$p_{ct}(i') = m(i')(p_{sc} + p_{dc}) + \frac{p_{out_1}}{v}, \tag{20}$$

where the output power of the active RIS, represented by p_{out_1}, is defined as $p_{out_1} = a_m^2 p_b ||\mathbf{h_{br}}||^2 + \sigma_2^2$.

Power consumption during D2D communications: Similarly, the active elements power consumption during D2D communications phase with the help of harvested energy is expressed as follows:

$$p_{ct}(i'') = m(i'')(p_{sc} + p_{dc}) + \frac{p_{out_2}}{v}, \tag{21}$$

where $p_{out_2} = a_m^2 \frac{e_{nl}(i')}{T(i'')} ||\mathbf{h_{sr}}||^2 + \sigma_2^2$,

3) RIS PANEL ENERGY CONSUMPTION

Overall RIS panel energy consumption during $T(i)$ is expressed as follows:

$$e_r(i) = \sum_{j \in \{i', i''\}} T(j)\big[p_{ss}(j) + p_{ct}(j)\big], \tag{22}$$

H. OPTIMIZATION PROBLEM

We formulate the optimization problem minimizing overall RIS elements' energy consumption subject to the information causality constraint, nonlinear energy harvesting model, and the number of RIS elements. The optimization problem, (**P**) is expressed as follows:

$$(\mathbf{P}) \quad \max_{m,k,p_b,T(i'),T(i'')} \Psi_1 B_b(i') - \Psi_2 e_r(i), \tag{23a}$$

$$\text{s.t. } m + k \le N, \tag{23b}$$

$$T(i') + T(i'') = T(i), \tag{23c}$$

$$\alpha_j \beta_j = 0, \ \forall j, \tag{23d}$$

$$e_{nl}(i^) = \frac{YT(i')}{1 + \exp(-y_1(p_{nl}(i') - y_2))}, \tag{23e}$$

$$e_r(i) = \sum_{j \in \{i', i''\}} T(j)\big[p_{ss}(j) + p_{ct}(j)\big], \tag{23f}$$

$$B_b = T(i')W_1 \log_2\left(1 + \frac{p_b\big(h_{bs} + m_k(i')h_1\big)^2}{\sigma_b^2}\right), \tag{23g}$$

$$T(i'')W_2 \log_2\left(1 + \frac{\frac{e_{nl}(i')}{T(i'')}\big(h_{sd} + m_k(i'')h_2\big)^2}{\sigma_d^2}\right) \ge B_b, \tag{23h}$$

The objective of the function is to maximize the number of BS-S bits, defined as $B_b(i')$ while minimizing the energy consumption of RIS elements, defined as $e_r(i)$, during $T(i)$, as described in (23a). Ψ_1 and Ψ_2 are constants, where $\Psi_2 - \Psi_1 < 0$. We optimize number of active, m, and passive elements, k in both phases, BS transmit power, p_b, and time $(T(i'), T(i''))$ for energy harvesting and D2D communications. The total number of active and passive elements is shown in (23b), where N is the maximum number of RIS elements used for designing the elements. The time constraint for energy harvesting, bits transmission from the BS to S, and D2D communications are shown in (23c). The amplitude for active and passive elements is described in (23d). The nonlinear constraint in (23e) defines the harvested energy from BS RF signals by S as no less than a threshold, e_m. The overall RIS panel energy consumption during $T(i)$ is shown in (23f), and the number of bits transmitted from the BS to S is shown in (23g), where $m_k(i) = \sum_{j \in \{i', i''\}} (a_m m(j) + k(j))$. The information causality constraint is defined in (23h). Solving the optimization problem is non-trivial, as (23) is a non-convex MINLP due to the coupling of optimizing variables, making it very difficult to solve optimally. Therefore, a heuristic solution approach is outlined in Section III to tackle the challenge.

III. SOLUTION TO (23)

The objective function in (23) describes a non-convex optimization problem, which is challenging to solve due to the interaction of the coupling variables in the objective function (23a), energy harvesting constraint (23e), data transmission constraint (23g), and the information causality constraint (23h). To simplify the complexity of (23), we break it into three smaller sub-problems and solve them in iteration. The first subproblem optimizes the RIS panel elements, given the BS transmit power and their corresponding time slots. The second subproblem uses the optimal RIS elements to optimize the time slots. The final subproblem optimizes the BS transmit power using the optimal elements and time slots. Each of the subproblems is investigated in turn in the following subsections. For clarity and ease of reading, we denote feasible points as $[\cdot]^f$ and optimal values as $[\cdot]^*$ in the remainder of this paper.

A. OPTIMAL RIS ELEMENTS, M^* AND K^*

$$\textbf{(P.A1)} \quad \max_{m,k} \ \Psi_1 B_b(i') - \Psi_2 \sum_{j\in\{i',i''\}} T(j)\big[p_{ss}(j)+p_{ct}(j)\big], \tag{24a}$$
$$\text{s.t. } m+k \le N, \tag{24b}$$
$$\alpha_j\beta_j = 0, \ \forall j, \tag{24c}$$
$$e_{nl}(i') = \frac{YT(i')}{1+\exp(-y_1(p_{nl}(i')-y_2))}, \tag{24d}$$
$$e_r(i) = \sum_{j\in\{i',i''\}} T(j)\big[p_{ss}(j)+p_{ct}(j)\big], \tag{24e}$$
$$B_b(i') = T(i')W_1\log_2\left(1+\frac{p_b\big(h_{bs}+m_k(i')h_1\big)^2}{\sigma_b^2}\right), \tag{24f}$$
$$T(i'')W_2\log_2\left(1+\frac{\frac{e_{nl}(i')}{T(i'')}\big(h_{sd}+m_k(i'')h_2\big)^2}{\sigma_d^2}\right) \ge B_b(i'), \tag{24g}$$

We optimize the number of active and passive elements in (24). We decouple the optimizing variables in $p_{ct}(i'')$ to solve the objective function in (24a). We, therefore, reformulate $p_{ct}(i'')$ as follows:

$$p_{ct}^f(i'') = m(i')(p_{sc}+p_{dc}) + \frac{\frac{a_m^2||\mathbf{h}_{\mathbf{sr}}||^2}{T(i'')}e_{nl}^f(i')+\sigma_2^2}{v}, \tag{25}$$

where

$$e_{nl}^f(i') = \frac{YT(i')}{1+\exp\left(-y_1\left(\zeta p_b\frac{\big(h_{bs}+m_k^f(i')h_1\big)^2}{\sigma_1^2}-y_2\right)\right)}, \tag{26}$$

and

$$m_k^f(i') = \Big(a_m m^f(i') + k^f(i')\Big), \tag{27}$$

Using (26), we redefine the information causality constraint as follows:

$$\log_2\Big(1+f_2\big(h_{sd}+(a_m m(i'')+k(i''))h_2\big)^2\Big)$$
$$\ge \log_2\Big(1+f_3\Big(h_{bs}+(a_m m^f(i')+k^f(i'))h_1\Big)^2\Big)^{f_1}, \tag{28}$$

where

$$f_1 = \frac{T(i'')W_2}{T(i')W_1}, \ f_2 = \frac{e_{nl}^f(i')}{\sigma_d^2 T(i'')}, \ f_3 = \frac{p_b}{\sigma_b^2}, \tag{29}$$

Using (28) and taking log term out, the following expression can be found:

$$\frac{\sqrt{\frac{f_3\big(h_{bs}+m_k^f(i')h_1\big)^{2f_1}}{f_2}}-h_{sd}}{h_2} \le a_m m(i'')+k(i''), \tag{30}$$

We reformulate the optimization problem as follows:

$$\textbf{(P.A2)} \quad \max_{m,k} \ \Psi_1 B_b(i') - \Psi_2 e_r^f(i), \tag{31a}$$
$$\text{s.t. } e_r^f(i) = T(i')p_{ct}(i') + T(i'')p_{ct}^f(i'') + \sum_{j\in\{i',i''\}} T(j)p_{ss}(j), \tag{31b}$$
$$B_b = T(i')W_1\log_2\left(1+\frac{p_b\big(h_{bs}+m_k(i')h_1\big)^2}{\sigma_b^2}\right), \tag{31c}$$
(24b), (24c), (26), (30)

Due to the coupling of variables m and k in $B_b(i')$, (31) is not convex yet. We also optimize the number of active and passive elements in (24). To make the expression a convex function, one approach is to use the first-order Taylor series expansion. This method approximates the non-convex function by a linear function at a specific point. Using this approach, we find a simpler expression that is both convex and reasonably approximates the original function. This approximation can be useful in solving the original problem or equation, as it allows us to use existing methods and algorithms that require convexity. Specifically, we approximate B_b by its first-order Taylor series expansion around a point (m_0, k_0) as follows:

$$B_b(m,k) \approx B_b(m_0,k_0) + \frac{\partial B_b(m_0,k_0)}{\partial m}(m-m_0) + \frac{\partial B_b(m_0,k_0)}{\partial k}(k-k_0), \tag{32}$$

where $\frac{\partial B_b(m_0,k_0)}{\partial m}$ and $\frac{\partial B_b(m_0,k_0)}{\partial k}$ are the partial derivatives of B_b with respect to m and k, evaluated at (m_0, k_0). This approximation can be used as a convex approximation of the original function and is useful in solving the original problem or equation. By using existing methods and algorithms that require convexity (justification is illustrated in Appendix B, we can obtain solutions that are reasonably close to the optimal solution of the original non-convex problem.

$$\begin{aligned} B_b^f &= W_1\log_2\left(1+\frac{p_b}{\sigma_1^2}\Big(h_{bs}+\Big(a_m m\big(i'\big)+k(i')\Big)h_1\Big)^2\right) \\ &\approx W_1\log_2\left(1+\frac{p_b}{\sigma_1^2}\Big(h_{bs}+\big(a_m m_0(i')+k_0(i')\big)h_1\Big)^2\right) \\ &\quad + W_1\frac{2p_b a_m h_1\Big(h_{bs}+\big(a_m m_0(i')+k_0(i')\big)h_1\Big)}{\sigma_1^2\ln 2\Big(1+p_b(h_{bs}+(a_m m_0(i')+k_0(i'))h_1)^2\Big)} \\ &\quad \Big(m(i')-m_0(i')\Big) \\ &\quad + W_1\frac{2p_b h_1\Big(h_{bs}+\big(a_m m(i')+k(i')\big)h_1\Big)}{\sigma_1^2\ln 2\Big(1+p_b(h_{bs}+(a_m m(i')+k(i'))h_1)^2\Big)} \\ &\quad \Big(k(i')-k_0(i')\Big), \end{aligned} \tag{33}$$

Finally, we rewrite the optimization problem as follows:

$$\textbf{(P.A3)} \quad \min_{m^*,k^*} \ \Psi_1 B_b^f(i') - \Psi_2 e_r^f(i). \tag{34}$$
s.t. (24b), (24c), (26), (30), (31b), (33)

where m^*, k^* are the optimal variables. Note that (34) is a convex problem. Feasible points, m^f and k^f are initialized to some reasonable random values. The feasible points are updated at every iteration until the optimal solutions, m^* and k^* are achieved. For the initialization of optimization problem **(P.A3)**, selecting reasonable random values for m^* and k^*, which represent the number of active and passive RIS elements respectively, requires consideration of the system's physical constraints and operational context. Given that m and k are constrained by the total number of RIS elements N (i.e., $m+k \leq N$), and both must be non-negative integers, we propose initializing these values within the range $[0, N]$. A uniform distribution could be utilized for this purpose, ensuring $0 \leq m, k \leq N$. If the sum of the initially selected m and k exceeds N, a proportional reduction can be applied to adhere to the total element constraint. This method ensures that the initial values are within a feasible range, respecting both the physical limitations of the RIS panel and the potential operational bias towards more active or passive elements depending on the system's specific requirements. For instance, if the total number of RIS elements is $N = 100$, one might start with values randomly selected from a uniform distribution over $[0, N]$ for both m and k, adjusting them proportionally if their sum surpasses N.

To solve problem **(P.A3)**, we employ an iterative Gradient Descent (GD) algorithm, well-suited for optimizing convex functions. The algorithm updates the RIS elements m and k iteratively by moving in the negative gradient direction of the objective function $\Psi_1 B_b^f(i') - \Psi_2 e_r^f(i)$, subject to the constraints. The update rule for each iteration is given by:

$$m^{(t+1)} = \text{Proj}\left(m^{(t)} - \alpha \frac{\partial}{\partial m}\left(\Psi_1 B_b^f\big(i'\big) - \Psi_2 e_r^f(i)\right)\right),$$
$$k^{(t+1)} = \text{Proj}\left(k^{(t)} - \alpha \frac{\partial}{\partial k}\left(\Psi_1 B_b^f\big(i'\big) - \Psi_2 e_r^f(i)\right)\right),$$

where α is the step size, and $\text{Proj}(\cdot)$ denotes the projection onto the feasible set defined by the constraints to ensure $m+k \leq N$. The algorithm iterates until convergence, defined by a small change in the objective function value between successive iterations.

B. OPTIMAL TIME SLOTS, $T^*(I')$ AND $T^*(I'')$

To obtain the optimal $T(i')$ and $T(i'')$, we need to reformulate (23) in terms of the parameters m^*, k^*, and p_b that are given. This can be reformulated as follows:

$$(\mathbf{P.B1}) \quad \max_{T(i'),T(i'')} \ \Psi_1 B_b\big(i'\big) - \Psi_2 e_r(i), \tag{35a}$$
$$\text{s.t. } T\big(i'\big) + T\big(i''\big) = T(i), \tag{35b}$$
$$e_{nl}\big(i'\big) = \frac{YT\big(i'\big)}{1+\exp(-y_1(p_{nl}(i') - y_2))} \tag{35c}$$
$$e_r(i) = \sum_{j\in\{i',i''\}} T(j)\big[p_{ss}(j) + p_{ct}(j)\big], \tag{35d}$$
$$B_b\big(i'\big) = T\big(i'\big) W_1 \log_2\left(1 + \frac{p_b\big(h_{bs} + m_k^*(i')h_1\big)^2}{\sigma_b^2}\right), \tag{35e}$$
$$T\big(i''\big) W_2 \log_2\left(1 + \frac{\frac{e_{nl}(i')}{T(i'')}\big(h_{sd} + m_k^*(i'')h_2\big)^2}{\sigma_d^2}\right) \geq B_b, \tag{35f}$$

We optimize time $(T(i'), T(i''))$ for energy harvesting and D2D communications, respectively. We redefine using optimal m^* and k^* for brevity as follows:

$$m_k^*(i) = \sum_{j\in\{i',i''\}} \big(a_m m^*(j) + k^*(j)\big), \tag{36}$$

We reformulate (35f) as follows:

$$T\big(i''\big) \log_2\left(1 + \frac{f_4}{T(i'')}\right) \geq T\big(i'\big) f_5, \tag{37}$$

where

$$f_4 = \frac{e_{nl}^f(i')}{\sigma_d^2}\big(h_{sd} + (a_m m^*(i'') + k^*(i''))h_2\big)^2, \tag{38}$$

$$e_{nl}^f\big(i'\big) = \frac{YT^f\big(i'\big)}{1+\exp(-y_1(p_{nl}(i') - y_2))}, \tag{39}$$

and

$$f_5 = \frac{W_1}{W_2} \log_2\left(1 + \frac{p_b\big(h_{bs} + \big(a_m m^*\big(i''\big) + k^*\big(i''\big)\big)h_1\big)^2}{\sigma_b^2}\right), \tag{40}$$

It is generally challenging to make convex (37). To find a convex lower bound for (37), using a convex relaxation technique, such as the log-sum-exp (LSE) [46].

Lemma 1: LSE function is a convex and continuously differentiable function commonly used in optimization.

Proof: Let $\mathbf{x} = (x_1, x_2, \ldots, x_n)$ be a vector of real numbers. Then, the LSE function is defined as:

$$\text{LSE}(\mathbf{x}) = \log\big[\exp(x_1) + \exp(x_2) + \cdots + \exp(x_n)\big], \tag{41}$$

LSE function is convex and continuously differentiable since the exponential function is convex, and taking the logarithm of a convex function preserves convexity. The expression for the derivative of the LSE function with respect to x_i is:

$$\frac{\partial}{\partial x_i}\text{LSE}(\mathbf{x}) = \frac{\exp(x_i)}{\exp(x_1) + \exp(x_2) + \cdots + \exp(x_n)}, \tag{42}$$

It is well-defined and continuous for all x_i as long as at least one exponent is positive.

The proof is complete. Using LSE, (37) can be used to approximate as follows:

$$T\big(i''\big) \log_2\left(e + \frac{f_4}{T(i'')}\right) \geq T\big(i'\big) f_5, \tag{43}$$

The convexity of the approximation in (43) enables us to optimize it using the LSE convex optimization technique. Therefore, we can reformulate the optimization problem as follows:

$$(\mathbf{P.B2}) \quad \max_{T(i'),T(i'')} \ \Psi_1 B_b\big(i'\big) - \Psi_2 e_r(i), \tag{44a}$$
$$\text{s.t. } e_r(i) = \sum_{j\in\{i',i''\}} T(j)\big[p_{ss}(j) + p_{ct}(j)\big], \tag{44b}$$
$$(43),\ (35c),\ (35b),\ (35e)$$

We also optimize time $(T(i'), T(i''))$ for energy harvesting and D2D communications, respectively. Note (44) is not a convex problem yet, primarily due to the presence of $p_{ct}(i'')$ in (44a) and (44b). To make it a convex problem, we introduce a feasible point and approximate the problem as follows:

$$p^f_{ct}(i'') = m^*(i'')(p_{sc} + p_{dc}) + \frac{a^2_m \frac{e^f_{nl}(i')}{T(i'')}}{v}||\mathbf{h_{sr}}||^2, \quad (45)$$

where

$$e^f_{nl}(i') = \frac{YT^f(i')}{1 + \exp(-y_1(p_{nl}(i') - y_2))}, \quad (46)$$

Finally, we can express the optimization problem as:

$$\textbf{(P.B3)} \quad \max_{T^*(i'),T^*(i'')} \Psi_1 B_b(i') - \Psi_2 e^f_r(i), \quad (47a)$$
$$s.t. e^f_r(i) = T(i')p_{ct}(i') + T(i'')p^f_{ct}(i'') + \sum_{j\in\{i',i''\}} T(j)p_{ss}(j). \quad (47b)$$
$$(43),\ (35c),\ (35b),\ (35e)$$

We can observe that (47) is a convex problem. We can initialize the feasible points $T^f(i')$ with some reasonable random values to solve this problem. At each iteration, we can update the feasible points using an appropriate algorithm until we obtain the optimal solutions $T^*(i')$ and $T^*(i'')$. The algorithm is designed to ensure that the feasible points are updated in a way that converges to the optimal values of $T^*(i')$ and $T^*(i'')$, thereby optimizing the objective function (47).

C. OPTIMAL BS TRANSMIT POWER, P^*_B

In this sub-section, we utilize optimal values for m^*, k^*, $T^*(i')$ and $T^*(i'')$ to attain the optimal BS power budget, denoted by p^*_b. To achieve this, we reformulate the optimization problem stated in (23) as follows:

$$\textbf{(P.C1)} \quad \max_{p_b} \Psi_1 B_b(i') - \Psi_2 e_r(i), \quad (48a)$$
$$\text{s.t. } e_{nl}(i') = \frac{YT^*(i')}{1 + \exp(-y_1(p_{nl}(i') - y_2))}, \quad (48b)$$
$$e_r(i) = \sum_{j\in\{i',i''\}} T(j)\left[p_{ss}(j) + p_{ct}(j)\right], \quad (48c)$$
$$B_b(i') = T^*(i')W_1 \log_2\left(1 + \frac{p_b\left(h_{bs} + m^*_k(i')h_1\right)^2}{\sigma^2_b}\right), \quad (48d)$$
$$\frac{T^*(i'')}{B_b(i')} W_2 \log_2\left(1 + \frac{\frac{e_{nl}(i')}{T^*(i')}\left(h_{sd} + m^*_k(i'')h_2\right)^2}{\sigma^2_d}\right) \geq 1, \quad (48e)$$

where we optimize BS transmit power, p_b. The exponential term of (48b) is dealt as follows:

$$p_b = \frac{\sigma^2_1\left(y_2 - \frac{\ln\left(\frac{YT^*(i')}{e_{nl}(i')} - 1\right)}{y_1}\right)}{\zeta\left(h_{bs} + (a_m m(i') + k(i'))h_1\right)^2}, \quad (49)$$

The optimization problem is rewritten as follows:

$$\textbf{(P.C2)} \quad \max_{p_b} \Psi_1 B_b(i') - \Psi_2 e_r(i), \quad (50a)$$
$$\text{s.t. } (48c),\ (48d),\ (48e),\ (49)$$

Optimizing variable is p_b. We rewrite (48e) as follows:

$$f_7 \geq \log_2(1 + f_6 p_b), \quad (51)$$

where

$$f_7 = \frac{T^*(i'')W_2}{T^*(i')W_1} \log_2\left(1 + e^f_{nl}(i')\frac{\left(h_{sd} + m^*_k(i'')h_2\right)^2}{T^*(i'')\sigma^2_d}\right), \quad (52)$$

$$f_6 = \frac{\left(h_{bs} + m^*_k(i')h_1\right)^2}{\sigma^2_b}, \quad (53)$$

and

$$e^f_{nl}(i') = \frac{YT^*(i')}{1 + \exp\left(-y_1\left(\zeta p^f_b \frac{(h_{bs}+m^*_k(i')h_1)^2}{\sigma^2_1} - y_2\right)\right)}, \quad (54)$$

Note that (51) is a concave function, meaning its second derivative is negative. To make it a convex function, we can take its negative, as the negative of a concave function is a convex function. Therefore, the following function is convex:

$$-\log_2(1 + p_b f_6) = -\log_2(1 + f_6 p_b)$$
$$= \log_2\left((1 + f_6 p_b)^{-1}\right) = \log_2\left(2^{-f_7} - f_6 p_b\right), \quad (55)$$

And the inequality can be written as: $\log_2(1 + f_6 p_b) \leq f_7$ which is equivalent to:

$$\log_2\left(2^{-f_7} - f_6 p_b\right) \geq 0, \quad (56)$$

The inequality is only true for values of $f_6 p_b$ that satisfy the constraint such that

$$\left(2^{-f_7} - f_6 p_b\right) > 0, \quad (57)$$

The optimization problem can be rewritten as follows:

$$\textbf{(P.C3)} \quad \max_{p_b} \Psi_1 B_b(i') - \Psi_2 e_r(i), \quad (58a)$$
$$\text{s.t. } e_r(i) = \sum_{j\in\{i',i''\}} T(j)\left[p_{ss}(j) + p_{ct}(j)\right], \quad (58b)$$
$$B_b(i') = T^*(i')W_1 \log_2\left(1 + \frac{p_b\left(h_{bs} + m^*_k(i')h_1\right)^2}{\sigma^2_b}\right), \quad (58c)$$
$$(49),\ (57)$$

Optimizing variable is also p_b. To obtain (33) and (58b), we make an approximation of (20) by assuming it to be convex, as shown below:

$$p^f_{ct}(i'') = m^*(i'')(p_{sc} + p_{dc}) + \frac{a_m^2 \frac{e^f_{nl}(i')}{T^*(i'')}||\mathbf{h_{sr}}||^2 + \sigma_2^2}{v}, \quad (59)$$

where

$$e^f_{nl}(i') = \frac{YT^*(i')}{1 + \exp\left(-y_1\left(\zeta p^f_b \frac{(h_{bs}+m_k(i')h_1)^2}{\sigma_1^2} - y_2\right)\right)}, \quad (60)$$

We rewrite the optimization problem as follows:

$$(\mathbf{P.C4}) \quad \max_{p_b^*} \Psi_1 B_b(i') - \Psi_2 e^f_r(i), \quad (61a)$$

$$\text{s.t. } e^f_r(i) = T^*\left(i'\right)p_{ct}\left(i'\right) + T^*\left(i''\right)p^f_{ct}\left(i''\right) + \sum_{j\in\{i',i''\}} T(j)p_{ss}(j). \quad (61b)$$

(58c), (49), (57)

where p_b^* is the optimal variable, i.e., optimal transmit power. Note (61) is a convex function. It can be solved using any standard optimization toolbox, which provides a range of algorithms to solve convex optimization problems. Therefore, the problem of optimizing (61) can be tackled using well-established and efficient optimization techniques, making the proposed solution efficient. In forthcoming studies, we delve into the intricacies of a bi-objective optimization model, enriching our analysis with a comprehensive array of optimal operational points. Such an approach is invaluable for mapping the Pareto frontier, articulating the trade-offs between energy efficiency and data rates in RIS-enhanced networks. We intend to provide network designers with a multi-faceted perspective, equipping them with the means to balance the competing demands inherent in IoT environments. The refined iterative algorithm will be adept at sifting through the complexity of multi-objective problems, yielding a versatile toolkit for meeting the dynamic requirements of contemporary communication systems.

D. PROPOSED ALGORITHM

To solve the formulated optimization problem, we use Algorithm 1, an iterative method that enables the efficient solving of the non-convex MINLP problem. Importantly, this algorithm allows various RIS elements, time allocation, and the BS transmit power to attain the optimization outcome. Algorithm 1 is given in the appendix and follows a series of steps crucial in enhancing the performance of RIS-assisted wireless networks. The iterative algorithm starts with initializing the values of Ψ_1, Ψ_2, m^f, k^f, $T^f(i')$, p^f_b, and ϵ to reasonable random values. Optimization begins with a repeat loop until the optimal value is found. In each iteration, the algorithm finds the optimal active and passive elements of the RIS using (34). The obtained optimal values m^* and k^* are then set as m^f and k^f, respectively. Next, the algorithm finds the optimal time slots, $T^*(i')$ and $T^*(i'')$, using (47), along with the values of m^* and k^*. The algorithm then updates the values of $T^f(i')$ to the new optimal values. After that, the algorithm finds the optimal transmit power of the BS, p_b^*, using (61), along with the optimal values of $T^*(i')$, $T^*(i'')$, m^* and k^*. The obtained optimal value p_b^* is then set as p^f_b. The repeat loop continues until the optimal values of m^*, k^*, $T^*(i')$, $T^*(i'')$, and p_b^* are found such that the difference between the previous and current iterations is less than ϵ. The algorithm aims to optimize the active and passive elements of the RIS, the time slots, and the BS iteratively transmit power until convergence is reached. The proposed algorithm is summarized in Algorithm 1.

Algorithm 1 Proposed Iterative Algorithm

```
Initialization: Ψ1, Ψ2, m^f, k^f, T^f(i'), p_b^f, and ϵ to some
  reasonable random values
Optimization:
repeat
    Determine m* and k*, by solving problem (P.A3).
    Set m^f = m* and k^f = k*
    Find T*(i') and T*(i'') using (P.B3), m* and k*
    Set T^f(i') = T*(i')
    Find p_b* using (P.C4), T*(i'), T*(i''), m* and k*
    Set p_b^f = p_b*
until Find the optimal value, such as m*, k*, T*(i'),
  T*(i''), and p_b* such that |x(l)| − |x(l − 1)| < ϵ, where
  x = m*, k*, T*(i'), T*(i''), p_b*
```

The main subproblems are RIS configuration optimization in Algorithm 1, energy harvesting optimization, and data transmission scheduling. The complexity of RIS configuration optimization is $\mathcal{O}(m)$, as there are m configurations. The complexity of energy harvesting optimization is $\mathcal{O}(n)$, as it involves a linear search through n devices. The last subproblem, data transmission scheduling, has a $\mathcal{O}(n^2)$ complexity due to the necessity of pairwise comparisons for optimal scheduling among n devices. The complexity of Algorithm 1 is connected to the number of IoT devices, n, and configurations of RISs, m. Its decomposition into three subproblems results in $\mathcal{O}(m + n + n^2)$, due to which the dominant value n^2, including data transmission scheduling, simplifies the entire complexity to $\mathcal{O}(n^2)$. This means that the algorithm's execution time refers to the square of the number of devices but is still sustainable for practical utilization in RIS-facilitated IoT networks.

IV. RESULTS

This section presents the simulation setup of the proposed model, including specific parameter details, and outlines the results. Our investigation focuses on stationary nodes, where their distances determine the gain between nodes. The channel gain is based on Rician fading, a commonly used model in wireless communications that accounts for both line-of-sight and non-line-of-sight components of signal propagation. The algorithms are simulated using a specific set of parameters, which include the thermal noise $\sigma^2 = -121.45$ dBm, amplification factor $a_m \in \{2.5, 3.0, 3.5\}$, RIS passive element power consumption $p_{sc} = -10$ dBm, RIS active element power consumption $p_{dc} = -5$ dBm. We use $W_1 = W_2 = 180$ KHz as the bandwidth of the carrier frequency. The energy efficiency factor and time are set as $\zeta \in \{0.20, 0.30, 0.40\}$ and $T(i) \in \{150, 200, 250, 300, 350\}$ ms, respectively. We assume wireless energy harvesting related constant Y to be 1, indicating that the maximum amount of power that can be charged is $1W$. We specify $y_1 = 1000$ to model circuit resistance and its associated losses, indicating notable resistance challenges in energy conversion efficiency. Conversely, $y_2 = 0.000002$ models capacitance and circuit sensitivity, reflecting high sensitivity and efficient energy fluctuation management, key for optimizing energy harvesting. The RIS panel, a key component of the proposed system, is designed with a minimum of 150 and a maximum of 500 elements. To solve the optimization performance, we use the GAMS tool [47], which is a high-level modeling system for mathematical programming and optimization. The parameter values selected for our simulations, including thermal noise level, amplification factor, RIS element power consumption, and bandwidth, were chosen to reflect real-world conditions and align with commonly used standards in RIS technology and IoT communications. This careful selection ensures that our simulation results are theoretically sound and practically relevant, enabling a realistic assessment of the system's performance across various RIS element counts.

The specific value of the amplification factor, a_m between 2.5 and 3.5 and a bandwidth of $180kHz$ are chosen in response to the operational constraints and technological specifics of existing RIS and IoT technologies. The arbitrary choice of the amplification factor is directly connected to the relationship between the noise of the amplification process and the thermal noise of RIS, thus guaranteeing the selection of feasible simulation parameters. Similarly, the bandwidth of 180 kHz agrees with the current NB-IoT standards, prioritizing IoT coverage's efficient and broad deployment. We have chosen to operate at a bandwidth of 180 kHz due to its prevalence in IoT applications, particularly in the sub-GHz frequency bands where many IoT devices operate.

In Fig. 3, the simulation results obtained by applying Algorithm 1 prove the suggested method's effectiveness in enhancing the IoT system's performance. The objective function increases within the first five iterations, and after that, it stabilizes and changes very little. This indicates the convergence of the algorithms, and the results produced by the algorithms are reliable. The fast convergence of Algorithm 1 is a desirable feature, as it indicates that Algorithm 1 can solve the problem efficiently and quickly. The energy harvesting varying over time is shown in Fig. 4. The higher efficiency factor guarantees higher energy harvesting in both algorithms. Specifically, the nonlinear energy harvesting model yields more energy. For example, with energy efficiency factor, $\zeta = 0.40$, compared to a lower

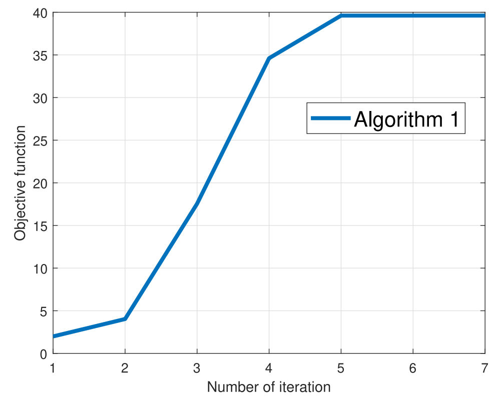

FIGURE 3. Convergence of Algorithm.

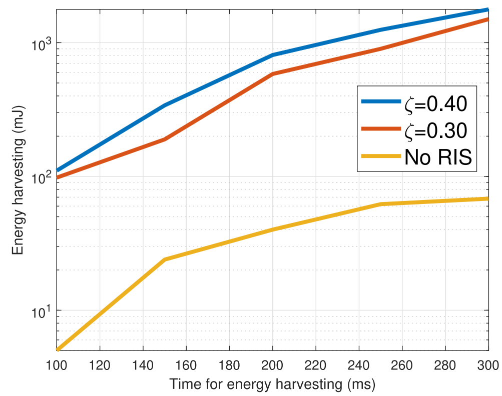

FIGURE 4. Energy harvesting varying over time.

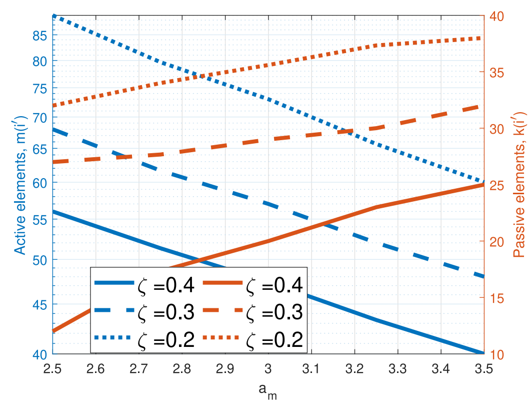

FIGURE 5. Elements during energy harvesting.

efficiency factor, such as $\zeta = 0.30$. Notably, the absence of the RIS panel in the networks leads to poor energy harvesting performance.

Fig. 5 and Fig. 6 illustrate the variation in the optimal number of active and passive elements required for energy harvesting from BS RF signals and D2D communications, respectively. The analysis aims to determine the optimal number of RIS elements by varying the amplification factor, a_m, for various values of ζ. The difference in the number of active and passive elements is due to the complexity of the energy harvesting from BS RF signals and D2D

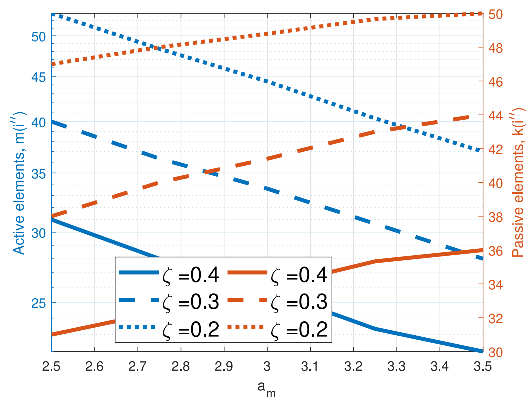

FIGURE 6. Elements during D2D communications.

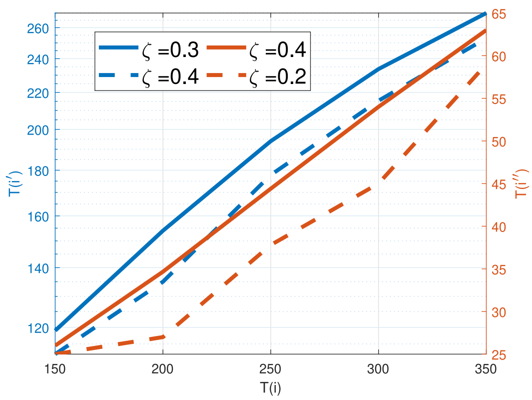

FIGURE 7. Time management.

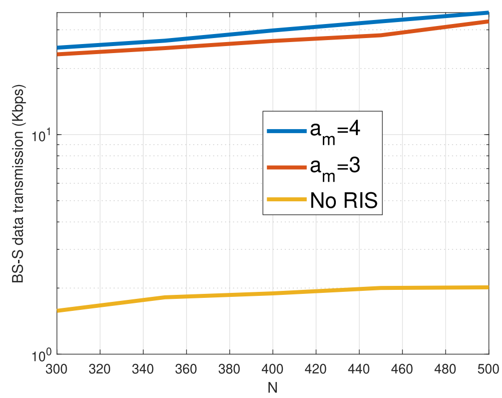

FIGURE 8. Information causality constraint: BS to S data transmission.

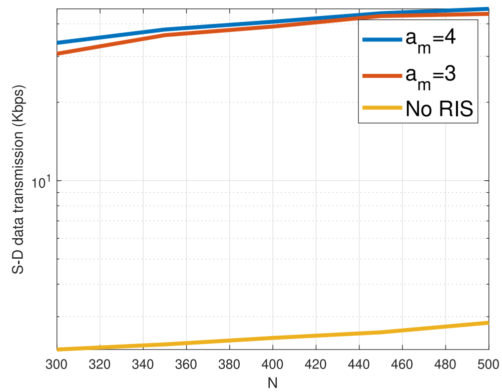

FIGURE 9. Information causality constraint: S to D data transmission.

communication processes. In both cases, the number of active elements decreases as a_m increases. For example, in Fig. 5, the active elements use 60% of the overall RIS elements; in Fig. 6, they use 34% of the overall RIS elements. Furthermore, the optimal number of passive elements slightly increases with an increase in the number of RIS elements. Specifically, for energy harvesting, the passive elements use only 21% of the overall RIS elements, while for D2D communications, they use 30% of the RIS elements. This difference in the percentage of passive elements used can be attributed to their role in each phase. In the energy harvesting phase, the active elements with higher a_m are crucial for achieving higher energy gain. In contrast, in D2D communications, passive elements play a significant role in reflecting and directing the signals between the communicating nodes. The optimal number of elements, indicated by the intersection points of the active and passive element curves in Fig. 5 and Fig. 6, represent the configurations where the system achieves a balance between energy harvesting and D2D communication efficacy. At these points, the system capitalizes on the trade-off between the enhanced directivity of active elements and the reduced thermal noise contribution from passive elements.

In Fig. 7, we observe the interplay between the efficiency factor ζ and the corresponding time allocations for energy harvesting $T(i')$ and D2D communications $T(i'')$. As ζ increases, denoting a more significant share of energy dedicated to harvesting, the optimal time for energy harvesting rises proportionally. At the same time, the time for D2D communications also increases but at a lesser rate. This allocation underscores the importance of optimizing ζ to balance the trade-off between energy collection and communication duration, which is crucial for the system's overall efficacy.

Fig. 8 and Fig. 9 show the data rate transmission using the RIS panel. To demonstrate the performance, we vary a_m for different numbers of RIS elements, such as $N \in \{300, 500\}$. We compare the RIS-assisted data rate with no RIS panel, and the proposed model shows an enhanced transmission rate of about 100% compared to the network without the RIS panel. It is reasonable to claim that the higher number of RIS elements results in a higher data rate. Comparing Fig. 8 and Fig. 9, we observe that the rate from S to D is higher or equal to the rate from BS to S, indicating that the information causality constraint is successfully applied to the network. This claim also holds when the system does not adopt any RIS panel, as the information causality constraint is independent of RIS. The initial selection of 300 RIS elements is based on prevalent RIS configurations in contemporary empirical studies. This benchmark facilitates an evaluation of RIS

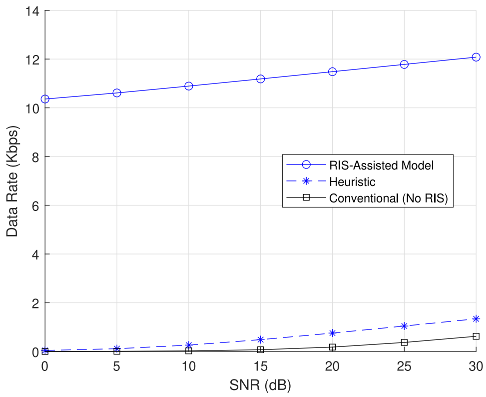

FIGURE 10. Data rate varying over SNR.

panel performance impacts within a range pertinent to current practical applications. The data presented also highlights the diminishing returns associated with integrating additional RIS elements, pointing to the necessity of identifying an optimal balance between enhanced system performance and the practicalities of resource allocation. It is important to note that the information causality constraint is consistently applied in our simulations, ensuring the system model's integrity regardless of the specific RIS panel implementation.

In Fig. 10, we present data rates of our proposed model with heuristic and conventional (No RIS) communication systems over varying SNR levels. Our model consistently outperforms the conventional approach, substantiating the efficacy of integrating RIS in enhancing data transmission rates. Fig. 10 also underscores the superiority of the proposed method over the heuristic strategy, especially at higher SNR values, highlighting the advantage of our optimized RIS configurations and signaling the significant potential of our approach in practical deployments.

V. CONCLUSION

This paper focuses on enhancing RIS-assisted wireless networks for b-IoT sensors. Previous literature primarily uses passive elements within RIS to boost performance, but our study underscores integrating both active and passive elements for optimization. This integration, however, can increase thermal noise, potentially limiting SNR improvement. We delve into the balance between RIS elements and system performance to augment RIS efficiency in wireless communications for b-IoT systems. Our investigation includes a practical scenario where a b-IoT sensor harvests energy from nearby BS RF signals during the first optimal time slot using a nonlinear energy harvesting model. Subsequently, the sensor transmits bits to another sensor, thereby improving D2D communications while adhering to an information causality constraint. Utilizing an RIS panel with both element types aids in both energy harvesting and D2D communications. We aim to maximize transmitted bits and minimize RIS power consumption within the constraints of our energy harvesting model. Identifying the optimal mix of RIS elements, time allocation, and BS transmit power. We address these challenges through an optimization problem considering the constraints of nonlinear energy harvesting and information causality. Iterative algorithms are employed to tackle this non-convex MINLP problem, demonstrating through simulations that RIS-assisted energy harvesting significantly improves IoT system performance over traditional benchmarks without RIS integration. Future work will extend this model to include BS with multiple antennas, aligning with more common real-world deployments and MIMO systems. It includes simulations that span a variety of channel conditions, ensuring that our analysis reflects the dynamic and stochastic nature of wireless channels.

APPENDIX A
PROOF OF CONVEXITY FOR THE DECOMPOSED SUBPROBLEMS

Given the optimization problem formulated as:

$$\max f(x) \text{ subject to } g_i(x) \leq 0, \text{ for } i = 1, \ldots, m \tag{62}$$

where $f(x)$ is the objective function and $g_i(x)$ are the constraint functions, the non-convex nature of the original problem (23) stems from the interaction between the variables in the objective function (23a) and the constraints (23e), (23g), and (23h). To demonstrate the convexity of the decomposed subproblems, we must show that the second derivative of the objective function $f(x)$ and each of the constraint functions $g_i(x)$ concerning the decision variables is non-negative. This can be established by the following: For the energy harvesting model, which involves a sigmoid function $\sigma(x) = \frac{1}{1+\exp(-ax)}$, it is known that:

$$\frac{d^2\sigma(x)}{dx^2} = a^2 \exp(-ax) \frac{\exp(-ax) - 1}{(1 + \exp(-ax))^3} \geq 0 \tag{63}$$

for $a > 0$. Thus, the energy harvesting model is convex. The objective function and constraints regarding the decision variables are linear for the data transmission scheduling. Given a linear function $h(x) = bx + c$, its second derivative is:

$$\frac{d^2h(x)}{dx^2} = 0 \tag{64}$$

Since the second derivative is zero, it indicates no curvature, and the function is thus convex.

APPENDIX B
QUANTITATIVE EVIDENCE

We present a quantitative analysis to justify our claim that convex optimization methods provide solutions that closely approximate the global optimum of the original non-convex problem. Our approach involves comparing the outcomes of convexified solutions with those obtained from global optimization techniques. We express as follows:

$$\max_{x \in \mathcal{X}} f(x), \quad \text{subject to} \quad g_i(x) \leq 0, \ i = 1, \ldots, m, \tag{65}$$

where $f(x)$ is a non-convex objective function, $g_i(x)$ represents the set of constraints, and $\mathcal{X}$ denotes the feasible region. We approximate (65) with a convex problem:

$$\max_{x\in\mathcal{X}} \tilde{f}(x), \quad \text{subject to} \quad \tilde{g}_i(x) \leq 0,\ i = 1, \ldots, m, \qquad (66)$$

where $\tilde{f}(x)$ and $\tilde{g}_i(x)$ are convex approximations of the objective function and constraints, respectively. To quantify the effectiveness of the convex approximation, we conducted experiments across N different scenarios, comparing the optimal solutions of the original non-convex problem, x^*_{global}, with the solutions obtained from the convex approximation, x^*_{convex}. For each scenario, we calculated the objective function value difference, $\Delta f = |f(x^*_{global}) - f(x^*_{convex})|$, and aggregated the results. The mean and standard deviation of Δf across all scenarios were computed to assess the closeness of the convex approximation to the global optimum. Our analysis reveals that the mean value of Δf falls within a tolerable margin, indicating that the convex approximation yields solutions remarkably close to the global optimum.

REFERENCES

[1] K. B. A. Bakar, F. T. Zuhra, B. Isyaku, and S. B. Sulaiman, "A review on the immediate advancement of the Internet of Things in wireless telecommunications," *IEEE Access*, vol. 11, pp. 21020–21048, 2023.

[2] S. N. Mahapatra, B. K. Singh, and V. Kumar, "A survey on secure transmission in Internet of Things: Taxonomy, recent techniques, research requirements, and challenges," *Arab. J. Sci. Eng.*, vol. 45, pp. 6211–6240, 2020.

[3] H. Rahmani et al., "Next-generation IoT devices: Sustainable eco-friendly manufacturing, energy harvesting, and wireless connectivity," *IEEE J. Microw.*, vol. 3, no. 1, pp. 237–255, Jan. 2023.

[4] D. Zorbas and C. Douligeris, "Computing optimal drone positions to wirelessly recharge IoT devices," in *Proc. IEEE Conf. Comput. Commun. Workshops (INFOCOM WKSHPS)*, 2018, pp. 628–633.

[5] J. Huang, Y. Zhou, Z. Ning, and H. Gharavi, "Wireless power transfer and energy harvesting: Current status and future prospects," *IEEE wireless Commun.*, vol. 26, no. 4, pp. 163–169, Aug. 2019.

[6] G. Vieeralingaam, R. Ramanathan, and M. Jayakumar, "Convex optimization approach to joint interference and distortion minimization in energy harvesting wireless sensor networks," *Arab. J. Sci. Eng.*, vol. 45, pp. 1669–1684, Mar. 2020.

[7] Z. Zhang, H. Pang, A. Georgiadis, and C. Cecati, "wireless power transfer—An overview," *IEEE Trans. Ind. Electron.*, vol. 66, no. 2, pp. 1044–1058, Feb. 2019.

[8] S. Ahmed, A. E. Kamal, and M. Y. Selim, "Adding active elements to reconfigurable intelligent surfaces to enhance energy harvesting for IoT devices," in *Proc. IEEE Mil. Commun. Conf. (MILCOM)*, 2021, pp. 297–302.

[9] S. Ahmed, M. Y. Selim, and A. E. Kamal, "Enhanced IoT batteryless D2D communications using reconfigurable intelligent surfaces," in *Proc. IEEE 47th Conf. Local Comput. Netw. (LCN)*, 2022, pp. 42–47.

[10] M. Jung, W. Saad, and G. Kong, "Performance analysis of active large intelligent surfaces (LISs): Uplink spectral efficiency and pilot training," *IEEE Trans. Commun.*, vol. 69, no. 5, pp. 3379–3394, May 2021.

[11] E. Basar, M. Di Renzo, J. De Rosny, M. Debbah, M.-S. Alouini, and R. Zhang, "Wireless communications through reconfigurable intelligent surfaces," *IEEE Access*, vol. 7, pp. 116753–116773, 2019.

[12] R. Long, Y.-C. Liang, H. Guo, G. Yang, and R. Zhang, "Symbiotic radio: A new communication paradigm for passive Internet of Things," *IEEE Internet Things J.*, vol. 7, no. 2, pp. 1350–1363, Feb. 2020.

[13] L.-G. Tran, H.-K. Cha, and W.-T. Park, "RF power harvesting: A review on designing methodologies and applications," *Micro Nano Syst. Lett.*, vol. 5, no. 1, pp. 1–16, 2017.

[14] N. A. Eltresy et al., "RF energy harvesting IoT system for museum ambience control with deep learning," *Sensors*, vol. 19, no. 20, p. 4465, 2019.

[15] A. Dhungana and E. Bulut, "Opportunistic wireless crowd charging of IoT devices from smartphones," in *Proc. IEEE 16th Int. Conf. Distrib. Comput. Sensor Syst. (DCOSS)*, 2020, pp. 376–380.

[16] D. Aashish and B. Eyuphan, "Energy balancing in mobile opportunistic networks with wireless charging: Single and multi-hop approaches," *Ad Hoc Netw.*, vol. 111, pp. 1023–42, Feb. 2021.

[17] S. Yin, E. Zhang, L. Yin, and S. Li, "Optimal saving-sensing-transmitting structure in self-powered cognitive radio systems with wireless energy harvesting," in *Proc. IEEE Int. Conf. Commun. (ICC)*, 2013, pp. 2807–2811.

[18] S. Lee, R. Zhang, and K. Huang, "Opportunistic wireless energy harvesting in cognitive radio networks," *IEEE Trans. Wireless Commun.*, vol. 12, no. 9, pp. 4788–4799, Sep. 2013.

[19] G. Zheng, Z. Ho, E. A. Jorswieck, and B. Ottersten, "Information and energy cooperation in cognitive radio networks," *IEEE Trans. Signal Process.*, vol. 62, no. 9, pp. 2290–2303, May 2014.

[20] J. Singh, R. Kaur, and D. Singh, "Energy harvesting in wireless sensor networks: A taxonomic survey," *Int. J. Energy Res.*, vol. 45, no. 1, pp. 118–140, 2021.

[21] A. Kurs, A. Karalis, R. Moffatt, J. Joannopoulos, P. Fisher, and M. Soljačić, "Wireless power transfer via strongly coupled magnetic resonances," *Science*, vol. 317, no. 5834, pp. 83–86, 2007.

[22] A. P. Sample, D. A. Meyer, and J. R. Smith, "Analysis, experimental results, and range adaptation of magnetically coupled resonators for wireless power transfer," *IEEE Trans. Ind. Electron.*, vol. 58, no. 2, pp. 544–554, Feb. 2011.

[23] H. Zhang and Z. Li, "Energy-aware data gathering mechanism for mobile sink in wireless sensor networks using particle swarm optimization," *IEEE Access*, vol. 8, pp. 177219–177227, 2020.

[24] H. J. Visser and R. J. Vullers, "RF energy harvesting and transport for wireless sensor network applications: Principles and requirements," *Proc. IEEE*, vol. 101, no. 6, pp. 1410–1423, Jun. 2013.

[25] M. S. Iqbal, Y. Sadi, and S. Coleri, "Minimum length scheduling for full duplex time-critical wireless powered communication networks," *IEEE Trans. Wireless Commun.*, vol. 19, no. 9, pp. 5993–6006, Sep. 2020.

[26] M. S. Iqbal, Y. Sadi, and S. Coleri, "Minimum length scheduling for discrete-rate full-duplex wireless powered communication networks," *IEEE Trans. Wireless Commun.*, vol. 21, no. 1, pp. 135–148, Jan. 2022.

[27] A. Zappone, M. Di Renzo, X. Xi, and M. Debbah, "On the optimal number of reflecting elements for reconfigurable intelligent surfaces," *IEEE Wireless Commun. Lett.*, vol. 10, no. 3, pp. 464–468, Mar. 2021.

[28] I. Yildirim, A. Uyrus, and E. Basar, "Modeling and analysis of reconfigurable intelligent surfaces for indoor and outdoor applications in future wireless networks," *IEEE Trans. Commun.*, vol. 69, no. 2, pp. 1290–1301, Feb. 2021.

[29] Z. Abdullah, G. Chen, S. Lambotharan, and J. A. Chambers, "A hybrid relay and intelligent reflecting surface network and its ergodic performance analysis," *IEEE Wireless Commun. Lett.*, vol. 9, no. 10, pp. 1653–1657, Oct. 2020.

[30] Z.-Q. He and X. Yuan, "Cascaded channel estimation for large intelligent metasurface assisted massive MIMO," *IEEE Wireless Commun. Lett.*, vol. 9, no. 2, pp. 210–214, Feb. 2020.

[31] P. Mursia, V. Sciancalepore, A. Garcia-Saavedra, L. Cottatellucci, X. C. Pérez, and D. Gesbert, "RISMA: Reconfigurable intelligent surfaces enabling beamforming for IoT massive access," *IEEE J. Sel. Areas Commun.*, vol. 39, no. 4, pp. 1072–1085, Apr. 2021.

[32] M. Nemati, J. Ding, and J. Choi, "Short-range ambient backscatter communication using reconfigurable intelligent surfaces," in *Proc. IEEE Wireless Commun. Netw. Conf. (WCNC)*, 2020, pp. 1–6.

[33] Z. Peng, Z. Zhang, C. Pan, L. Li, and A. L. Swindlehurst, "Multiuser full-duplex two-way communications via intelligent reflecting surface," *IEEE Trans. Signal Process.*, vol. 69, pp. 837–851, Jan. 2021.

[34] L. Liu, R. Zhang, and K.-C. Chua, "Wireless information transfer with opportunistic energy harvesting," *IEEE Trans. Wireless Commun.*, vol. 12, no. 1, pp. 288–300, Jan. 2013.

[35] S. Luo, R. Zhang, and T. J. Lim, "Optimal save-then-transmit protocol for energy harvesting wireless transmitters," *IEEE Trans. Wireless Commun.*, vol. 12, no. 3, pp. 1196–1207, Mar. 2013.

[36] S. Li, B. Duo, X. Yuan, Y.-C. Liang, and M. Di Renzo, "Reconfigurable intelligent surface assisted UAV communication: Joint trajectory design and passive beamforming," *IEEE Wireless Commun. Lett.*, vol. 9, no. 5, pp. 716–720, May 2020.

[37] R. Alhamad, "Throughput and detection probability of interweave cognitive radio networks using intelligent reflecting surfaces," *Arab. J. Sci. Eng.*, vol. 47, pp. 1–12, Mar. 2022.

[38] K. Ntontin et al., "Toward autonomous reconfigurable intelligent surfaces through wireless energy harvesting," 2021, *arXiv:2108.07953*.

[39] A. C. Tasolamprou et al., "Exploration of intercell wireless millimeter-wave communication in the landscape of intelligent metasurfaces," *IEEE Access*, vol. 7, pp. 122931–122948, 2019.

[40] C. Liaskos, S. Nie, A. Tsioliaridou, A. Pitsillides, S. Ioannidis, and I. Akyildiz, "Realizing wireless communication through software-defined hypersurface environments," in *Proc. IEEE 19th Int. Symp, World Wireless Mobile Multimedia Netw. (WoWMoM)*, 2018, pp. 14–15.

[41] H. Sun, Q. Wang, S. Ahmed, and R. Q. Hu, "Non-orthogonal multiple access in a mmWave based IoT wireless system with SWIPT," in *Proc. IEEE 85th Veh. Technol. Conf.*, 2017, pp. 1–5.

[42] J. Joung, C. K. Ho, K. Adachi, and S. Sun, "A survey on power-amplifier-centric techniques for spectrum-and energy-efficient wireless communications," *IEEE Commun. Surveys Tuts.*, vol. 17, no. 1, pp. 315–333, 1st Quart., 2014.

[43] R. Long, Y.-C. Liang, Y. Pei, and E. G. Larsson, "Active reconfigurable intelligent surface-aided wireless communications," *IEEE Trans. Wireless Commun.*, vol. 20, no. 8, pp. 4962–4975, Aug. 2021.

[44] J. Lee and K. Yang, "RF power analysis on 5.8 GHz low-power amplifier using resonant tunneling diodes," *IEEE Microw. Wireless Compon. Lett.*, vol. 27, no. 1, pp. 61–63, Jan. 2017.

[45] F. Amato, C. W. Peterson, B. P. Degnan, and G. D. Durgin, "Tunneling RFID tags for long-range and low-power microwave applications," *IEEE J. Radio Freq. Identif.*, vol. 2, no. 2, pp. 93–103, Jun. 2018.

[46] M. J. Neely, "Energy optimal control for time-varying wireless networks," *IEEE Trans. Inf. Theory*, vol. 52, no. 7, pp. 2915–2934, Jul. 2006.

[47] "GAMS." Accessed: Dec. 2021. [Online]. Available: https://www.gams.com/